Analytical Methods

ROYAL SOCIETY OF CHEMISTRY

TECHNICAL NOTE

View Article Online
View Journal | View Issue

Cite this: *Anal. Methods*, 2024, **16**, 6570

Savitzky–Golay processing and bidimensional plotting of current–time signals from stochastic blocking electrochemistry to analyze mixtures of rod-shaped bacteria†

Ashley Tubbs,[a] Junaid U. Ahmed,[b] Jayani Christopher[a] and Julio C. Alvarez *[a]

In stochastic blocking electrochemistry, adsorptive collisions of nano and micro-particles with an ultramicroelectrode (UME) generate steps of decreasing current overlaid on the current–time (*i*–*t*) baseline of an electroactive mediator reacting at the UME. The step amplitude (Δ*i*) induced by particle blockage informs about its size, while collision frequency correlates with particle transport. However, because most particles arrive at the UME faster than the acquisition speed of conventional electrochemical instruments, current steps appear vertical. Recently, when analyzing rod-shape bacteria (bacilli), we detected slanted steps of duration Δ*t* (~0.6 to 1.1 s) that were found to scale up with bacillus length (~1 to 5 μm, respectively). In this work, we apply a Savitzky–Golay (SG) algorithm coded in MATLAB to convert experimental *i*–*t* recordings into derivative plots of Δ*i*/Δ*t versus t*. As a result, current steps become peaks on a flat baseline. Unlike the original values of Δ*i* and Δ*t* that require manual gauging, the coded SG-algorithm generates both parameters automatically from peak integration. We then display Δ*i* and Δ*t* in bidimensional scatter plots comparing mixtures of *A. erythreum* (~1 μm) and *B. subtilis* (~5 μm). The spread of Δ*i* and Δ*t* values complies with the size distribution observed using scanning electron microscopy. By introducing SG-processing and bidimensional plotting of *i*–*t* recordings from stochastic blocking data we broaden the scope of the technique. The approach facilitates distinguishing bacilli in mixtures because both Δ*t* and Δ*i* increase with bacillus length and now they can be displayed in a single graph along with adsorption frequency. Moreover, density distribution and proportion of data points from groups of bacteria are also discernible from the plots.

Received 14th May 2024
Accepted 30th August 2024

DOI: 10.1039/d4ay00899e

rsc.li/methods

Introduction

Of the electrochemical techniques that detect single particle impacts,[1–4] stochastic blocking electrochemistry remains the most universal because it can probe both insulating[5,6] and conductive particles.[7] In this technique, colliding particles disrupt the flux of an electroactive mediator reacting at the surface of an ultramicroelectrode (UME). Individual adsorptive impacts appear as steps of decreasing current (Δ*i*) overlaid on the baseline of current–time (*i*–*t*) for the mediator steady-state response.[1,5,6] Particle size affects the magnitude of Δ*i*, while collision frequency is controlled by particle concentration and transport.[1] However, because data acquisition in conventional electrochemical instruments is slower than the collision speed of most particles,[5,8] current steps appear vertical.[5,6] Consequently, since the first report on stochastic blocking electrochemistry in 2004,[1] the main focus has been on understanding how Δ*i* relates to particle size,[5,6] and the ways that transport and concentration affect collision frequency.[9–12] Hence, research on extracting particle information from the transient character of current steps has been scarce.[13,14] Recently, when examining adsorptive impacts of rod-shaped bacteria (bacilli), we detected slanted current steps (Scheme 1)

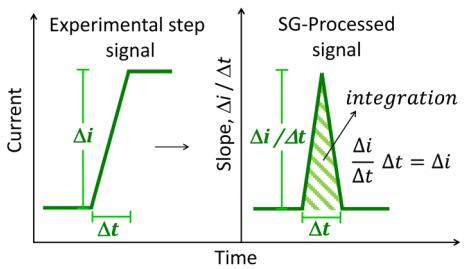

Scheme 1 Representation of signal processing by a 1st-derivative SG-filter applied to current steps of magnitude Δ*i* and duration Δ*t* from *i*–*t* recordings of adsorptive impacts of bacilli on UMEs. Both Δ*i* and Δ*t* are obtained automatically upon integration.

[a]*Chemistry Department, Virginia Commonwealth University, Richmond, VA, 23284, USA. E-mail: jcalvarez2@vcu.edu*

[b]*Chemistry Department, Khulna University of Engineering and Technology, Bangladesh*

† Electronic supplementary information (ESI) available: MATLAB script. See DOI: https://doi.org/10.1039/d4ay00899e

that exhibited a duration Δt, proportionate to bacillus length.[14] In this work, we extend that investigation to exploit Δt using digital processing of *i*–*t* recordings from bacilli mixtures. We created a MATLAB script (see ESI†) that applies a Savitzky–Golay (SG)[15] algorithm to experimental *i*–*t* recordings and generates Δi and Δt values automatically. We then prepared bidimensional plots of Δi and Δt for binary mixtures of bacilli. The analysis scope of the technique broadens because even in mixed populations of bacteria, Δi, Δt, and adsorption frequency can be displayed in a single graph. To the best of our knowledge this is the first time a SG-filter is applied to *i*–*t* recordings from stochastic blocking electrochemistry to render bidimensional scatter plots of current and time data points.

Since their development in 1964,[15] SG digital filters have been applied to data processing in various fields, including infrared spectroscopy,[16] medicine,[17] and geosciences.[18] SG-filters work by fitting a range of adjacent data points in a signal (*i.e.* wavelength, time, *etc.*) to a least-squares polynomial value.[15] The latter becomes a weighted average for the center point of the data interval.[15] Each data point in the signal is replaced by a local polynomial fit as the SG-filter moves through successive adjacent intervals to render a smoothed output of the initial signal.[15] The data range and order of the polynomial are chosen beforehand. A lesser-known feature of SG-filters relies on obtaining the derivative of the polynomial to yield smoothed derivative plots of pristine signals.[15] We applied the latter approach to experimental *i*–*t* recordings and produced plots of $\Delta i/\Delta t$ *versus* t (Scheme 1). As a result, current steps become peaks on a flat baseline, and values of Δi and Δt are generated from peak integration (Scheme 1). Both values of Δi and Δt are obtained automatically and take less time to extract than manual measurement from *i*–*t* recordings. Moreover, when Δi and Δt are plotted in bidimensional charts, mixtures of bacteria can be examined graphically, as is done using dot plots obtained from flow cytometry.[19–21] The latter is a technology that interrogates single cells employing laser beams when cells flow in solution.[19] Chemical and physical information from cell populations is visualized in bidimensional dot plots according to fluorescent or light scattering characteristics from individual cells. Here we make similar plots, displaying Δi and Δt as proxies of bacillus length.[14] When comparing mixtures of *A. erythreum* (~1 μm) and *B. subtilis* (~5 μm), we find that variations in Δi and Δt, reflect the dispersity of size distribution observed using scanning electron microscopy.

Our goal here was to develop new ways of extracting information from *i*–*t* recordings in stochastic blocking electrochemistry after having detected the new parameter Δt.[14] By combining SG-filtering and bidimensional plotting of Δi and Δt, we expand the scope of this technique to differentiate bacilli by rod length. This processing approach newly applied to stochastic blocking electrochemistry can be extended to other rod-shaped bacteria given that bacilli are responsible for serious infections like, tuberculosis, tetanus, typhoid, diphtheria, anthrax, salmonellosis, and several more.[22] Moreover, spherical microbial cells like yeast, can also be analyzed because as we demonstrated recently, they exhibit rather long Δt-values due their large size.[23]

Materials and methods

Reagents

All reagents were used as received without further purification. Potassium hexacyanoferrate(II) trihydrate ($K_4[Fe(CN)_6]$), (98.5%), sodium chloride, sodium phosphate dibasic, and potassium phosphate monobasic were obtained from Sigma-Aldrich (St. Louis, MO, USA). Potassium chloride (KCl) was purchased from Thermo Fisher Scientific (Hampton, NH, USA). All aqueous solutions were prepared using Millipore water (≥18.2 MΩ cm).

Instrumentation

All electrochemical experiments were performed using a CHI 660C potentiostat (CH Instruments, Austin, TX, USA) with a three-electrode setup in a single-compartment electrochemical cell housed in a Faraday cage. The electrode setup comprised a 3 M Ag/AgCl reference electrode, Pt wire counter electrode, and a Pt working ultramicroelectrode (UME) fabricated as described in prior literature (10.7 ± 0.1 μm disk diameter).[24] Before and between experiments, the Pt UME was gently polished with 0.05 μm alumina powder (Buehler, Lake Bluff, IL, USA) slurry on a Buehler polishing pad. Scanning electron microscopy (SEM) was completed using a Hitachi SU-70 FE-SEM operating at 5 kV. Critical drying of samples in preparation for SEM was achieved using an Autosamdri-931 (Rockville, MD, USA). Dynamic light scattering (DLS) experiments were performed using a ZetaSizer Nano ZS (Malvern Panalytical, Westborough, MA, USA).

Cell culturing and bacteria preparation

Luria–Bertani (LB) broth was prepared by adding 10 g of tryptone, 5 g of yeast extract, and 10 g of NaCl to 1 L of water. The LB broth was the autoclaved for 45 minutes prior to use for cell culturing. A 100 μL-aliquot of 50% glycerol stock solution containing *Aeromicrobium erythreum* or *Bacillus subtilis* was added to 10 mL of LB broth and grown in a rotary shaker at 37° for 24 hours (*B. subtilis*) or 48–72 hours (*A. erythreum*). Cell growth was monitored using optical density measurements and only bacteria in the stationary phase were used to perform experiments.[25]

The concentration of the bacterial cells was calculated using optical density measurements. Cells were harvested by centrifuging 1 mL of the cell culture at 3500 rpm for 5 minutes (*B. subtilis*) or 5000 rpm for 8 minutes (*A. erythreum*).[26] The supernatant was removed and the pellet was resuspended in 1 mM PBS. The solution was centrifuged again before resuspending the cells in a solution of 100 mM $K_4[Fe(CN)_6]$ and 1 mM KCl. All vials, tubes, and pipette tips were stored on a clean bench and cell cultures were stored in a sealed vial to avoid contamination.

Scanning electron microscopy

Cells in liquid media were centrifuged and washed in PBS solution twice, then resuspended in 1 mL of 3% glutaraldehyde and refrigerated for 24 hours to preserve cell morphology. After

refrigeration, the glutaraldehyde solution was removed by centrifuging the cells three times with PBS, then dehydrated by suspending the cells in a series of ethanol–water solutions from 30 to 100% ethanol. After dehydration, the cells were drop-casted onto clean silicon wafers followed by critical point drying. The silicon wafers were then fixed to conductive carbon tape and coated with gold for SEM imaging.

Data collection and analysis

Electrochemical experiments were recorded using CH Instrument's CHI660 software version 18.01. Data analysis was performed using a homemade MATLAB (R2019a) script (ESI†) to calculate step magnitude, Δi, and duration, Δt. Steps were manually counted and analyzed to confirm the accuracy of the MATLAB script.

Results and discussion

Experimental *i–t* response

Fig. 1B shows the *i–t* response for 100 mM of $Fe(CN)_6^{4-}$ and 1 mM KCl (without *B. subtilis*), while the potential of the UME was kept at +0.40 V *vs.* Ag/AgCl. This potential was chosen to attain a steady-state current wherein ferrocyanide oxidation becomes limited by mass transport.[14,27] The concentration of cells was adjusted to 10 fM (Fig. 1B) using the same ferrocyanide solution for the bacillus-free response. In contrast to the blank trace, the *i–t* curve for bacilli shows single adsorption events manifested as current steps (Fig. 1B inset) over the baseline of ferrocyanide oxidation.[14] Despite appearing upwards, the steps represent drops in current,[14] which arise from bacteria blocking ferrocyanide flux at the UME surface as observed in previous studies.[12,14,28–30] Even though the landing locus on the UME surface influences the magnitude of current steps,[6] bacillus length and particle size in general, also control Δi-values.[14] The frequency of adsorption (number of steps per second) is regulated by bacillus concentration and transport mode.[1,10] We and others, have demonstrated that transport to the UME surface for bacteria is dominated by electromigration.[14,30] The positive potential imposed to oxidize $Fe(CN)_6^{4-}$, pulls the negatively charged cells towards the UME, with a velocity compatible with electromigration,[14] including some contribution from electroosmosis.[12] The negative charge of the cells was confirmed by measuring zeta potential values of -41 ± 6 and -36 ± 5 mV for *B. subtilis* and *A. erythreum*, respectively (see Materials and methods). The low concentration of supporting electrolyte (KCl) also causes electromigration of ferrocyanide, which affects the magnitude of the steady-state current as we have shown previously,[14] however the conclusions of this work remain the same.

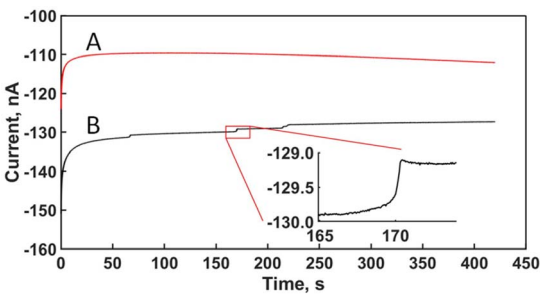

Fig. 1 *i–t* response on a disk-Pt UME of ~10 μm in diameter held at +0.4 V *vs.* Ag/AgCl, 100 mM $Fe(CN)_6^{4-}$, 1 mM KCl. (A) No cells; (B) steps (inset) for individual adsorptive collision of *B. subtilis* (10 fM) appear upwards but represent drops in current baseline.

Application of first derivative Savitzky–Golay filter

Though SG-smoothing appears in the MATLAB tools, the algorithm to apply the 1st derivative filter does not, therefore we created a script (see ESI†) to carry out the calculation steps described in the original paper by Savitzky and Golay.[15] Typically, a SG-filter is applied to the signal of interest by selecting an interval of data points (Scheme 2) equal to an odd number (11 for this case). The center point of this interval is replaced by a value from polynomial fitting using convolution coefficients listed in the original paper by Savitzky and Golay for a data set of 11.[15] Then, the interval shifts one data point over (Scheme 2) to calculate the next center value and continue the iteration until all values in the signal are replaced by polynomial fits.

We chose a range of 11 data points so that $2m + 1$ is equal to 11 and $m = 5$ (Scheme 2). Then, we took the convolution coefficients (C_k) and normalization factor (N) corresponding to the 1st derivative and the quadratic (2nd order) polynomial to fit the 11 points from the original table by Savitzky and Golay.[15] The SG-derivative filter calculates a new value using eqn (1) to replace the center data point of the moving window.[15] In this expression, each data point of experimental *i–t* plots is represented by y_j in the *y*-axis (current) and Δx_j in the *x*-axis (time). The latter is written as an interval because SG-filters are applied to equidistant points in the *x*-axis,[15] which for *i–t* plots corresponds to the sampling interval employed during acquisition (0.05 s). Because current steps in Fig. 1 are defined by Δi and Δt, the fitted values calculated using eqn (1) constitute a derivative $\Delta i/\Delta t$ (slope) of the corresponding data points in a *i–t* recording.

$$\text{Slope} = \sum \frac{C_k y_{j+k}}{\Delta x_j N} \quad (1)$$

The index k goes from m to $-m$, the limits of the moving window, while j (1, 2, 3, …, n) designates data point order. Once the first value is fitted, the window moves one data point over, along the data set to fit the next value.

This process continues iteratively until replacing all data points in a *i–t* recording. Fig. 2 illustrates the transition from

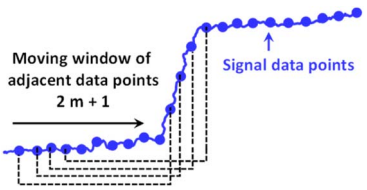

Scheme 2 Pictorial representation of a SG-filter being applied to a *i–t* step signal. The moving window of adjacent data points is selected so that $2m + 1$ is equal to an odd number, in this case 11 ($m = 5$).

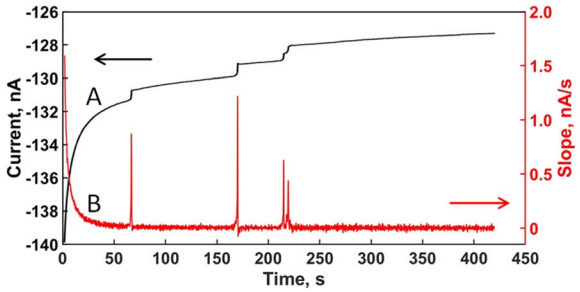

Fig. 2 (A) i–t recording for *B. subtilis* in Fig. 1; (B) slope plot ($\Delta i/\Delta t$) after applying a 1st-derivative SG-filter using a 11-point data interval ($2m + 1 = 11$, $m = 5$).

Table 1 Comparison of values from i–t and derivative plots[a]

Δi		Δt	
i–t plot	Derivative	i–t plot	Derivative
0.423	0.403	2.142	1.637
0.221	0.211	1.468	1.518
0.138	0.142	2.099	1.872
0.327	0.312	1.174	0.845
0.078	0.101		

[a] From Fig. 2.

the experimental i–t plot (Fig. 2A) to the SG-derivative plot (Fig. 2B). Every step in the i–t plot becomes a peak on the relatively flat baseline of the derivative plot. Several advantages arise from the transformation: (1) peaks are easier to discern than steps, especially when appearing close together like the steps between 200 and 250 s in Fig. 2A; (2) peak integration

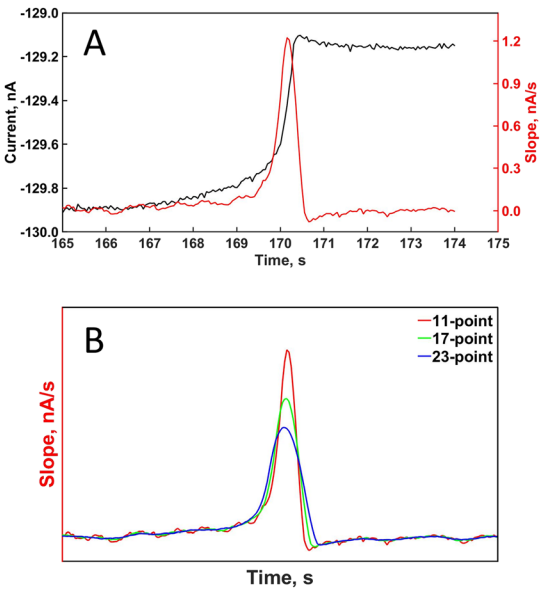

Fig. 3 (A) Comparison of a step and a derivative peak illustrating the challenge of integrating and extracting Δi and Δt from a step; (B) effect of the number of adjacent points used to calculate the slope points in the derivative plot.

renders the parameters Δi and Δt automatically (Scheme 1). (3) Processing of a i–t plot with multiple steps is quicker and produces similar values from manual estimates (Table 1).

Fig. 3A overlays a step with its corresponding derivative peak to illustrate that it is easier to integrate a peak than a step, because in the former the baselines match. We found that when increasing the number of data points in the "processing window", the peaks come out slightly broadened their base while decreasing their height (Fig. 3B). Such result led us to select the 11-point window for processing the i–t plots in this work because the peaks appeared heightened and the values of Δi and Δt extracted were closer to the manual estimates.

Analysis of binary mixtures of bacilli

Bidimensional plots of unmixed and mixed bacilli are shown in Fig. 4. To collect the data and prepare the plots, collision experiments with 10 fM of each bacillus (*A. erythreum* and *B. subtilis*) were run in separate electrochemical cells. The resulting i–t curves were processed using the SG-derivative filter and plotted together in Fig. 4A. Another series of experiments was performed with 10 fM of each bacillus mixed in the same solution. After SG-derivative these data are plotted in Fig. 4B. The boxes in Fig. 4A were drawn by calculating the overall average of Δi and Δt across trials and data points, adding the standard deviation on both sides (vertical or horizontal) of the average value to delineate the box perimeter. We copied and

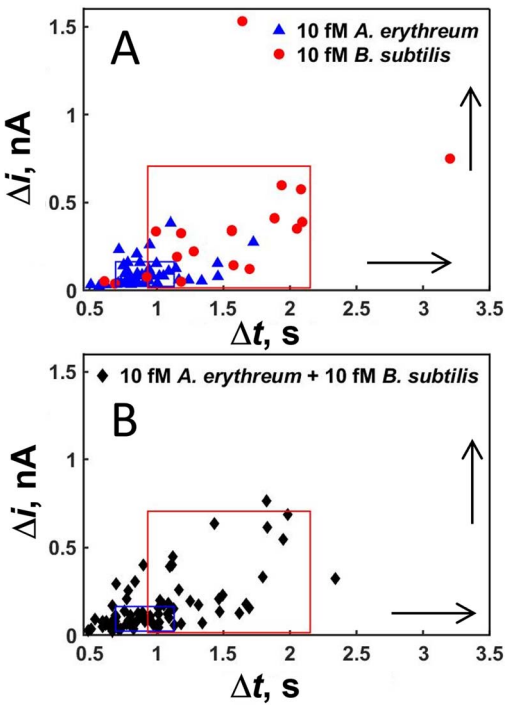

Fig. 4 Bidimensional plots of Δi and Δt values after SG-processing for *B. subtilis* and *A. erythreum* (10 fM each). The arrows indicate the direction wherein Δi and Δt cue bacillus length increments. (A) Plotted together from separate i–t experiments with boxes delineating standard deviations of Δi and Δt for each bacillus. (B) Mixed bacilli in one i–t experiment using the boxes from (A) to identify bacilli in the mixed sample.

pasted the boxes from Fig. 4A and B as an attempt to identify the bacilli in the mixed sample. However, the boxes represent a visual aid to identify the two groups of bacteria, given their wide and overlapping distributions of Δi and Δt values. Had the ranges been narrower, they would appear as separate data clusters distinguishable from one another, each representing a population in the mixture. Bacteria are expected to show broad size distributions because they engage in a constant cycle of birth and death. We believe this lack of discriminative power in Fig. 4, can be addressed by adding a dilute polymer hydrogel that slows down bacterial arrival due to viscosity and differential permeation.

We believe the bidimensional representation in Fig. 4 brings benefits because it can display values of Δi and Δt for mixed samples and enables potential identification of cell groups by size, given that both parameters increase when bacillus length grows.[14]

Previously, we found that the longer the rod length of the bacillus, the larger the distance from the UME surface at which ferrocyanide flux begins to be disrupted during cell arrival, thereby generating a heighted value of Δt.[14] Similarly, based on experiments and simulations,[27] Δi has been found to be proportional to the bare electrode current, i_B, and the square of the ratio, r_p/r_e, following the empirical expression:[27,31]

$$\Delta i = i_B \left(\frac{r_p}{r_e}\right)^2 \quad (2)$$

Here, r_p symbolizes the radius of a spherical particle, and r_e corresponds to the radius of the UME. Eqn (2) is only approximate because it does not consider the flux difference between center and edge that distinguishes UMEs.[27] Consequently, eqn (2) or a variant of it can only be used if the landing location of the particle on the UME is known.[32] Nevertheless, given that both Δi and Δt behave as proxies for bacillus length (see arrows in Fig. 4), they can still be used to analyze bacterial samples using the bidimensional plots in Fig. 4. In cases where size distributions are narrow, cells groups would be identifiable by their location on the bidimensional chart.

The degree of scattering observed for Δi and Δt in Fig. 4 results from the broad size distribution exhibited by *B. subtilis* and *A. erythreum*. Fig. 5 shows images from scanning electron microscopy for both bacilli. The distributions obtained from surveying the cells in the images are also depicted in Fig. 5. Overlap of the boxes in Fig. 4 can be explained by the wide range of sizes shown by these bacteria.

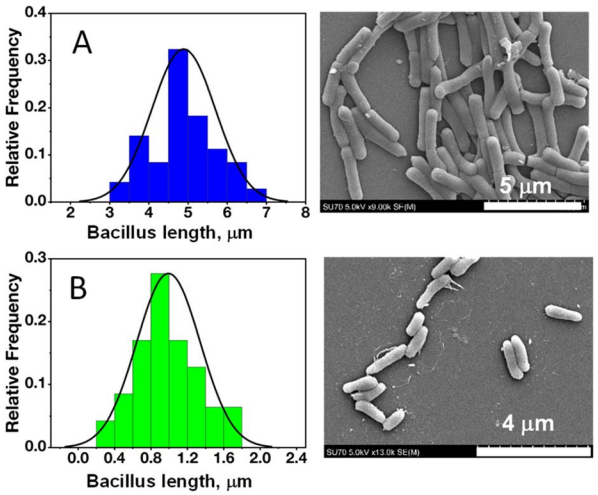

Fig. 5 Scanning electron micrographs and rod-length distribution for (A) *B. subtilis* and (B) *A. erythreum*.

Conclusions

We have described a method that enables analysis of bacterial populations using bidimensional plots of Δi and Δt from i–t recordings in stochastic blocking electrochemistry. Because both parameters grow when bacillus length increases, we can use data distribution on the plot to compare and in some cases distinguish populations of bacteria. This is despite lacking formulae that relate Δi and Δt with bacillus size. We arrived at this method by applying a SG-derivative filter that converts current steps from experimental i–t plots to peaks on a flat baseline. We carry out the method using a home-made MATLAB script that delivers Δi and Δt automatically from peak integration. Both parameters show similar values to Δi and Δt manually extracted from i–t plots. Combining SG-filtering and bidimensional plotting of Δi and Δt, we expand the scope of this technique to differentiate bacilli using rod length. This processing approach may be applicable to other microbial and mammalian cells, provided their current steps in i–t recordings exhibit measurable Δt-values. It is important to realize that this technique is applicable only to low concentration samples (fM to pM) because simultaneous bacterial collisions blur data interpretation, similar to single molecule measurements that use diffraction-limited optics wherein nanomolar concentrations overload the detector.[33] Therefore, concentrated samples would have to be diluted.

The present approach has the sensitivity of single cells, emulating methods like electron microscopy, coulter counting, AFM, flow cytometry, and fluorescence microscopy, but requires less instrumental complexity and footprint. Selectivity relies purely on bacterium size, but discrimination in mixtures remains challenging because of the intrinsic broad distributions displayed by bacteria. We believe that dissolving a polymer hydrogel in solution to provide differential permeability during bacterial collisions may help narrow the bidimensional distributions of Δi and Δt and discriminate bacteria in mixtures. Another way consists in applying signal correlation analysis[34] to the i–t plots and use the collision frequency as fingerprint for size. We will try these ideas in upcoming work.

Data availability

The data supporting this article have been included as part of the ESI.†

Author contributions

A. Tubbs conceived the idea, conducted experiments and digital processing, curated data, prepared figures, and wrote an initial draft of the paper; J. U. Ahmed obtained microscopy data; J. Christopher cultured cells; J. C. Alvarez wrote final manuscript draft and curated data. All authors reviewed the manuscript.

Conflicts of interest

There are no conflicts to declare.

Acknowledgements

Research funds from a Catalyst Award 2021 by VCU are greatly appreciated. A. T. acknowledges generous financial support from VCU through a Dissertation Assistantship Award. J. U. A. thanks Altria for a Graduate Research Fellowship and financial support from the Chemistry Department at Khulna University of Engineering and Technology in Bangladesh.

References

1 B. M. Quinn, P. G. van't Hof and S. G. Lemay, Time-Resolved Electrochemical Detection of Discrete Adsorption Events, *J. Am. Chem. Soc.*, 2004, **126**, 8360–8361.
2 X. Xiao and A. J. Bard, Observing Single Nanoparticle Collisions at an Ultramicroelectrode by Electrocatalytic Amplification, *J. Am. Chem. Soc.*, 2007, **129**, 9610–9612.
3 Y. G. Zhou, N. V. Rees and R. G. Compton, The Electrochemical Detection and Characterization of Silver Nanoparticles in Aqueous Solution, *Angew. Chem., Int. Ed.*, 2011, **50**, 4219–4221.
4 J. Poon, C. Batchelor-McAuley, K. Tschulik and R. G. Compton, Single Graphene Nanoplatelets: Capacitance, Potential of Zero Charge and Diffusion Coefficient, *Chem. Sci.*, 2015, **6**, 2869–2876.
5 A. Boika, S. N. Thorgaard and A. J. Bard, Monitoring the Electrophoretic Migration and Adsorption of Single Insulating Nanoparticles at Ultramicroelectrodes, *J. Phys. Chem. B*, 2013, **117**, 4371–4380.
6 S. E. Fodsdick, M. J. Anderson, E. G. Nettleton and R. M. Crooks, Correlated Electrochemical and Optical Tracking of Discrete Collision Events, *J. Am. Chem. Soc.*, 2013, **135**, 5994–5997.
7 J.-H. Park, A. Boika, H. S. Park, H. C. Lee and A. J. Bard, Single Collision Events of Conductive Nanoparticles Driven by Migration, *J. Phys. Chem. C*, 2013, **117**, 6651–6657.
8 D. A. Robinson, M. A. Edwards, H. Ren and H. S. White, Effects of Instrumental Filters on Electrochemical Measurement of Single-Nanoparticle Collision Dynamics, *ChemElectroChem*, 2018, **5**, 3059–3067.
9 Z. Deng and C. Renault, Detection of Individual Insulating Entities by Electrochemical Blocking, *Curr. Opin. Electrochem.*, 2021, **25**, 100619.
10 S. G. Lemay, C. Renault and J. E. Dick, Particle Mass Transport in Impact Electrochemistry, *Curr. Opin. Electrochem.*, 2023, **39**, 101265.
11 T. Moazzenzade, X. Yang, L. Walterbos, J. Huskens, C. Renault and S. G. Lemay, Self-Induced Convection at Microelectrodes via Electroosmosis and its Influence on Impact Electrochemistry, *J. Am. Chem. Soc.*, 2020, **142**, 17908–17912.
12 S. N. Thorgaard, S. Jenkins and A. R. Tarach, Influence of Electroosmotic Flow on Stochastic Collisions at Ultramicroelectrodes, *Anal. Chem.*, 2020, **92**, 12663–12669.
13 J. H. Chung, J. L. Jiseon, J. Hwang, K. H. Seol, K. M. Kim, J. Song and J. Chang, Stochastic Particle Approach Electrochemistry (SPAE): Estimating Size, Drift Velocity, and Electric Force of Insulating Particles, *Anal. Chem.*, 2020, **92**, 12226–12234.
14 J. U. Ahmed, J. A. Lutkenhaus, A. Tubbs, A. Nag, J. Christhopher and J. C. Alvarez, Estimating Particle Arrival Velocities Using the Time Variation of the Current Signal in Stochastic Blocking Electrochemistry, *Anal. Chem.*, 2022, **94**, 16560–16569.
15 A. Savitzky and M. J. E. Golay, Smoothing and Differentiation of Data by Simplified Least Squares Procedures, *Anal. Chem.*, 1964, **36**, 1627–1639.
16 A. Rinnan, Pre-processing in Vibrational Spectroscopy – When, Why and How, *Anal. Methods*, 2014, **6**, 7124–7129.
17 M. Unal, R. Ahmed, A. Mahadevan-Jansen and J. S. Nyman, Compositional Assessment of Bone by Raman Spectroscopy, *Analyst*, 2021, **146**, 7464–7490.
18 I. G. Roy, An Optimal Savitzky-Golay Derivative Filter with Geophysical Applications: An Example of Self-Potential Data, *Geophys. Prospect.*, 2020, **68**, 1041–1056.
19 E. Zand, A. Froehling, C. Schoenher, M. Zunabovic-Pichler, O. Schlueter and H. Jaeger, Potential of Flow Cytometric Approaches for Rapid Microbial Detection and Characterization in the Food Industry - A Review, *Foods*, 2021, **10**, 3112–3155.
20 L. A. Herzenberg, J. Tung, W. A. Moore, L. A. Herzenberg and D. R. Parks, Interpreting Flow Cytometry Data: A Guide for the Perplexed, *Nat. Immunol.*, 2006, **7**, 681–685.
21 E. Lugli, M. Roeder and A. Cossarizza, Data Analysis in Flow Cytometry: The Future Just Started, *Cytometry, Part A*, 2010, **77**, 705–713.
22 R. Sliman, S. Rehm and D. Shlaes, Serious Infections Caused by Bacillus Species, *Medicine*, 1987, **66**, 218–223.
23 J. A. Lutkenhaus, J. U. Ahmed, M. Hasan, D. C. Prosser and J. C. Alvarez, Average Collision Velocity of Single Yeast Cells During Electrochemically Induced Impacts, *Analyst*, 2024, **149**, 3214–3223.
24 J. U. Ahmed, J. A. Lutkenhaus, M. S. Alam, I. Marshall, D. K. Paul and J. C. Alvarez, Dynamics of Collisions and Adsorption in the Electrochemistry of Individual Emulsion Microdroplets, *Anal. Chem.*, 2021, **93**, 7993–8001.
25 J. A. Myers, B. S. Curtis and W. R. Curtis, Improving Accuracy of Cell and Chromophore Cocentration Measurements Using Optical Density, *BMC Biophys.*, 2013, **6**, 4.

26 B. W. Peterson, P. K. Sharma, H. C. van de Mei and H. J. Busscher, Bacterial Cell Surface Damage Due to Centrifugal Compaction, *Appl. Environ. Microbiol.*, 2012, **78**, 120–125.

27 A. J. Bard, L. R. Faulkner and H. S. White, *Electrochemical Methods: Fundamentals and Applications*, Wiley, New York, 3rd edn, 2022.

28 G. Gao, D. Wang, R. Brocenschi, J. Zhi and M. V. Mirkin, Toward the Detection and Identification of Single Bacteria by Electrochemical Collision Technique, *Anal. Chem.*, 2018, **90**, 12123–12130.

29 J. Y. Lee, B. K. Kim, M. Kang and J.-H. Park, Label-Free Detection of Single Living Bacteria via Electrochemical Collision Event, *Sci. Rep.*, 2016, **6**, 30022.

30 A. T. Ronspees and S. N. Thorgaard, Blocking Electrochemical Collisions of Single E. coli and B. subtilis bacteria at Ultramicroelectrodes Elucidated Using Simultaneous Fluorescence Microscopy, *Electrochim. Acta*, 2018, **278**, 412–420.

31 J. E. Dick, C. Renault and A. J. Bard, Observation of Single-Protein and DNA Macromolecule Collisions on Ultramicroelectrodes, *J. Am. Chem. Soc.*, 2015, **137**, 8376–8379.

32 J. Bonezzi and A. Boika, Deciphering the Magnitude of Current Steps in Electrochemical Blocking Collision Experiments and Its Implications, *Electrochim. Acta*, 2017, **236**, 252–259.

33 D. S. White, M. A. Smith, B. Chanda and R. H. Goldsmith, Strategies for Overcoming the Single-Molecule Concentration Barrier, *ACS Meas. Sci. Au*, 2023, **3**, 239–257.

34 Y. W. Lee, T. P. Cheatham and J. B. Wiesner, Application of Correlation Analysis to the Detection of Periodic Signals in Noise, *Proc. Inst. Radio Eng.*, 1950, 1165–1171.

